RPD

Revista Produção e
Desenvolvimento

MACHINABILITY OF PURE METALS
BY ELECTRICAL DISCHARGE MACHINING

P.M.H.Sousa[1*]; I.Bragança[2]; A.Jesus[3]; J.Marafona[3] e P.Rosa[1]
1 IDMEC, Departamento de Engenharia Mecânica, Instituto Superior Técnico, Universidade de Lisboa, Portugal
2 Departamento de Engenharia Mecânica, Instituto Superior de Engenharia de Lisboa, Portagal
3 Departamento de Engenharia Mecânica, Faculdade de Engenharia da Universidade do Porto, Portugal

*pedro.horta.sousa@gmail.com

ABSTRACT

Electrical discharge machining (EDM) involves the generation of micro-plasmas subjected to high temperature and pressure to promote the material removal. Hence, to understand the material removal mechanism it is of great importance the knowledge of the interaction plasma-solid. Knowing how physical and chemical properties of materials affect heat transfer at the electrode surface, how this eventually affects electrical properties of the plasma channel over the discharge time are key issues to achieve a better understanding of this machining technology. This research attempts to provide some answers to these issues by means of single plasma discharge tests under laboratory-controlled conditions carried out on pure and low-alloyed materials in favour of comprehensiveness and forthcoming numerical modelling. These results demonstrate that material eroded volume is correlated with process operating parameters and that crater morphology has presented a more regular shape in pure metals than in engineering materials. The machinability index of the materials under study has been determined by calculations of the eroded volume and electrical power measures. Further to the low predictability of the models presented in literature, it was also proposed a basic conceptual model referring to the morphology of the eroded craters.

KEYWORDS: electrical discharge machining, crater morphology, machinability, pure metals

1. INTRODUCTION

Electrical discharge machining (EDM) has become a key non-traditional technology widely used to machine high geometric and dimensional accuracy components in a broad spectrum of low and high-alloyed metals, and others conductive materials (Lu, 2007). Material removal occurs due to complex thermo-physical phenomena taking place in the gap between tool electrode and workpiece in the presence of a dielectric fluid surrounding environment. Pulsed electrical discharges have a melting-evaporation effect and wrap an erosive layer around the tool shape that is copied into the part with an offset equal to the gap between the electrode and the workpiece (Kunieda, 2005). Although EDM has been broadly implemented in current industrial scene, its fundamentals are still not well understood, promoting the use of empirical technological charts (Shumacher, 2004). Even with the scientific community interest that EDM has gained in recent years there is not a general agreement about the material removal mechanism, because there is a great lack of knowledge about the influence of certain operational parameters in the erosion process. One of the major reasons for this is because of the difficulty in perceiving the material removal mechanics which takes place in a very small ($\sim10^{-5}$m) overheated ($\sim10^{4}$K) gap between electrodes at transient conditions ($\sim10^{-5}$s) on a high occurrence frequency basis ($\sim10^{5}$Hz). In general, the study of the EDM process is carried out on commercial machine tools (multi-discharge) involving different discharge types that occur simultaneously at transient conditions. This lack of control and monitoring is not fully compatible with a comprehensive analysis on how the operating conditions affect heat transfer at the electrode surface and how erosion of workpiece occurs (Braganca, 2013).

As discussed by Eubank (Eubank, 1993), the mechanics of material removal in electrical discharge machining combines several phenomena from different fields of expertise, such as (i) electrical plasma discharges, (ii) thermodynamics, (iii) metallurgy and, surprisingly, (iv) materials strength. Hence, to understand the material removal mechanism it is of great importance to know how thermo-mechanical and electrical properties change with the operating conditions over the discharge time and how this eventually affects the heat transfer at the electrodes surface. The performance of the process is also affected by alterations in the electrical properties of the medium, caused by variations in the working parameters such as temperature, pressure, among others. Abdulkareem (Abdulkareem, 2009) concluded that cryogenic machining of titanium alloys changes the materials electrical and thermal conductivities, and thereby minimizes its melting and vaporization, reducing the wear of the electrode and improve the surface roughness. Liu (Liu, 2013) concluded that the increase in temperature (from $\sim25^{\circ}$C to $\sim70^{\circ}$C) in the machining of mould steel it promotes a decrease in the material removal rate and electrode wear rate. The authors suggest that this result can be explained by a decrease in the dielectric viscosity. These effects contribute to change the mechanisms of material removal (Zhang, 2011).

The theoretical modelling of EDM is still in its infancy, and it requires a fundamental level of understanding about the generation of micro-plasmas and its action on the solid materials (Kanemaru, 2011) and (Schumacher, 2004). Calibration of the input data remains an obvious shortcoming of the theoretical modelling, in order to assist the selection of process parameters in view of obtaining surfaces with excellent quality, high removal rates, and low tool wear. Therefore, the present research is intended to provide some reference boundaries for the physical parameters required to evaluate forthcoming numerical simulation performance of the electrical discharge machining process. This can only be achieved through laboratory-controlled experiments using pure metals with well-defined thermo-mechanical and electrical properties, such as melting temperature, electrical resistivity, specific heat, among others. The overall presentation is supported by specially designed point-to-plane electrical discharge experiments, performed on low-alloyed metallic materials and pure metals test specimens. Results have focused eroded craters morphology resulting

from the plasma-solid interaction and its correlation with the main operating parameters. It will be demonstrated that while the crater diameter is significantly influenced by the pulse time and electrical current, the crater depth is less sensitive to the variation of the operating parameters. The Reynaert's index predicts the machinability of the testing materials quite well, while the use of pure metals promotes regular geometries for the eroded crater.

2. REMOVAL MECHANISM AND ERODED CRATER MORPHOLOGY

According to the literature, electrical discharge machining can be structured in three major phases such as (i) ionization of the medium (dielectric fluid) and formation of the plasma channel, (ii) electrical discharge and (ii) extinction of the plasma channel. The first stage concerns the breakdown phenomenon leading to the creation of a spark that consists in a very rapid growth of a thin weakly-ionized channel called streamer (Figure 1). The streamer is typical formed between two electrodes from an intensive electron avalanche, starting from the cathode. This electric field increases with the avalanche propagation and avalanche has to reach certain amplification before it can create a streamer. When the avalanche reaches a certain value equal to or greater than the external field and if the density of the liquid is not high, a micro-vapour bubble is formed, where the streamer will start within the same. Depending on the values of the gap and the voltage, it can be created positive or negative streamers. Then controlling the location of the eroded crater on the machined surface. Once the streamer is started, it spreads and grows due to the random nature of its propagation mechanism. (Descoeudre, 2006)
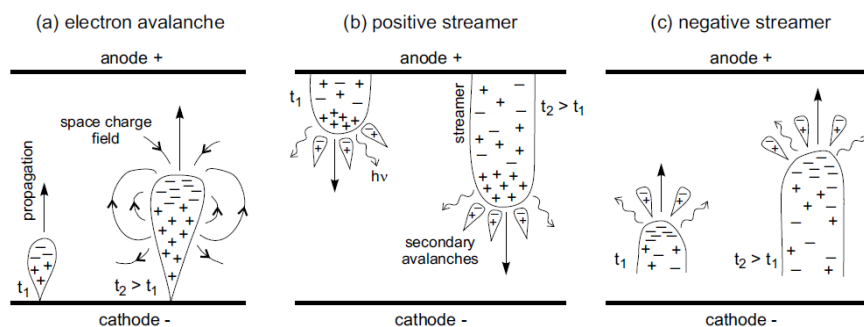
Figure 1 - Breakdown mechanisms leading to an electrical discharge.
Fonte: (Descoeudre, 2006).

The second phase of the process comprises the electric discharge between the two electrodes where the pressure, current intensity and temperature are maximum. Then, a solid-plasma interaction through the electric discharge promotes the removal of material (Figure 2). The discharge energy, given by Equation 1, is quantifiable function of the voltage, V(t), the intensity of the current, I(t), and discharge time, t_a. At a low current, a small quantity of heat is generated and a substantial portion of it is absorbed by the surroundings and the eroded surface, the left of it is utilized in melting and vaporizing the work material. But as the current is increased, a stronger spark with higher energy is produced, more heat is generated and a substantial quantity of heat is utilized in material removal. Material removal rate (MRR) can be approximated by the ratio between the variation in workpiece volume and pulse time (Khan, 2011). Also, the physical properties of the materials used as electrode and workpiece have to be taken into account, since, the physical properties influence a larger or smaller MRR. The physical properties of the materials influence the difficulty or facility of the machining. In 1997, Reynaerts (Reynaerts, 1997) proposed an equation that quantifies the machinability of materials by EDM (index of machinability, C_m).

The properties that Reynaerts considered essential for the calculation of this index (Equation 2) are: the specific heat, c (J/m^3.K), the thermal conductivity, λ (W/K.m), and the melting point, T_m (K), being the index quite affected by the last one since in the equation it is raised squared. Materials with a high erosion index can be used as tool electrodes, while materials with a low resistance index are used as workpiece material.
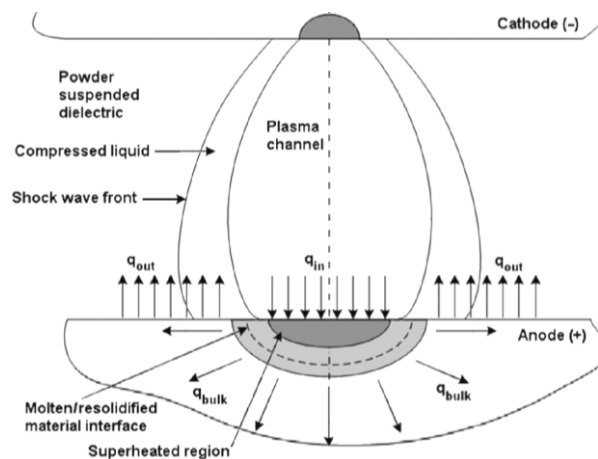
Figure 2 - Schematic representation of heat exchanges in plasma-solid interaction during an electric discharge.
Fonte: (Yeo, 2008)

$$W = \int_0^{ta} V(t)\,I(t)\ dt \qquad [Eq.\ 1]$$

$$C_m = \lambda \cdot c \cdot T_m^2 \qquad [Eq.\ 2]$$
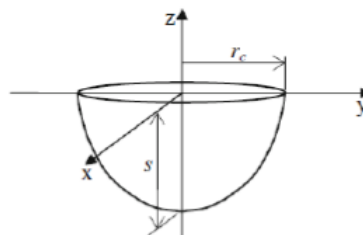
Figure 3 - Half spherical calotte model.
Source: (Salonitis, 2009).

In the third and final phase, the electrical pulse is extinguished and the conducting plasma channel is no longer formed. Molten material is consequently ejected and eroded debris are washed by the action of a fresh and deionizes dielectric flow. All that remains is the eroded crater. Considering the literature within the framework of theoretical modelling the morphology of the eroded craters can be approximated to a half spherical calotte. This type of geometry was developed taking into account point-to-plane type simplifications (heat point-source) (Dibitonto, 1989). More recently, authors such as Salonitis (Salonitis, 2009) or Popa (Popa, 2009), also claim that eroded craters can be represented by the half spherical decay model (Figure 3). However, experimental observations under laboratory controlled conditions have showed that eroded craters have a less slender geometry, and its shape resembles more a smooth bowl shape. This was confirmed by Bragança (Bragança, 2013a) after several single pulse discharge tests.

3. MATERIALS AND METHODS

This work uses a dedicated testing machine that produces single point-to-plane spark discharges in a dielectric medium, allowing for a free independent selection of the main operation parameters. The single spark tests have been complemented with the three-dimensional survey of the obtained eroded craters through chromatic confocal microscopy. In what follows, it will be presented the materials and methods involved in the experimental research.

3.1. Experimental Apparatus

Figure 4 shows an specifically designed testing machine that creates single point-to-plane spark discharges for a free selection of operation parameters and monitors the electrical signature during each discharge. This machine was designed, fabricated, and instrumented by the authors and consists of (i) basic structural and kinematic appliances, (ii) power supply module, (iii) load transducer module, and (iv) data acquisition and controller unit. This is the second version of the machine described in (Bragança, 2013b), which was improved in several aspects such as the power supply circuit and the positioning control devices. The tank is designed to securely fix the workpiece and to allow submersing it during the tests. This tank is assembled on the worktable which is anchored directly on the intermediate baseplate. The positioning control devices of the machine (Figure 4.a) comprise a servomechanism (Z axis servo head) based on a double-parallel screw-drive actuator driven by two stepper motors (200 steps), connected to a stepper-motor driver board (based in the Allegro A4988 chip). The first one (Z_1 axis) is a screw-drive actuator for fast positioning of the tool electrode in the testing area, while the second (Z_2 axis) allows a high precision resolution of $0.042\mu m$ (for 1/16 step). The tool block slide mounts directly on the machine column and accepts the tool holder (Figure 4.b). This set allows an adjustable feed rate at maximum resolution for a 25mm displacement.
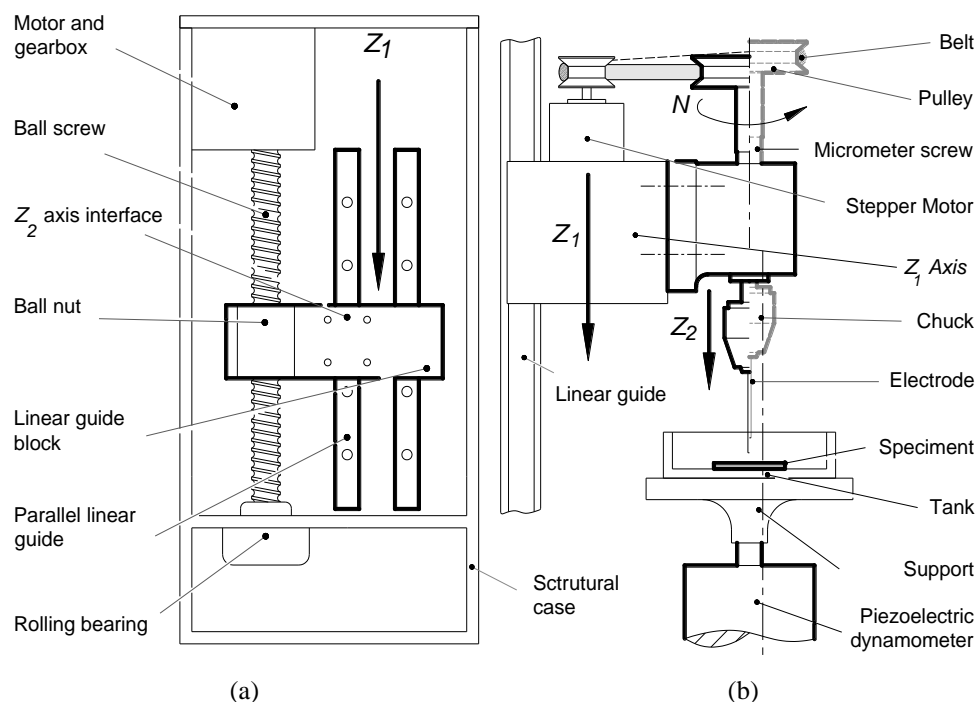
Figure 4 - Single discharge testing machine; (a) Schematic representation of the basic structural and kinematics appliances, and (b) high precision screw drive-actuator and load sensor.
Source: Elaborated by the authors (2016).

Specific electrical and electronic circuits include the power supply module, the control module, the data acquisition module and specific transducers that provide the monitoring of physical parameters, as shown in Figure 5. Each of these modules includes several electrical and electronic components. The power supply module consists of a variable voltage transformer, a constant-current bridge rectifier for converting the single-phase AC-supplied voltage into a DC voltage in the range 20V to 310V, and a bank of capacitors with 3300µF and current rating up to 30A. A MOSFET and several variable purely resistive components are used to control the electrical excitation pulse. The MOSFET behaves as a switch that closes and opens the discharge circuit, by supplying the control voltage (square pulses) and the pulse duration through the main board. The power supply device behaves like a purely resistive pulse generator. A PC-based data logging has the double purpose of providing data acquisition of process parameters and controlling the testing machine during the experiments. This system is based on a National Instruments NI-PCI-6070E data acquisition card. The electrical parameters (voltage and current) are measured by Hameg HZ100 voltage transducer and Bergoz CTB1 current transducer. These signals are transmitted through an oscilloscope (Tektronix 2004B) to the PC, to prevent lag time and support real-time data survey. The control module provides two types of control: (i) it defines the gap between the electrodes and (ii) it controls and monitors the plasma electrical parameters. This system is based on a custom-written software using LabVIEW from National Instruments. The DAQ makes use of expected operation parameters for acting on the tool positioning servomechanism and the electronic setting of the power supplier. The feedback signals obtained from voltage and current sensors allow a precise adjustment of the (frontal) gap between electrodes. Figure 6.a) shows the experimental apparatus used during the investigation and Figure 6.b) the testing machine where it is possible to see a micrometer with a ratio of 500µm/rev, being driven by a stepper motor being possible to control the value of the gap.
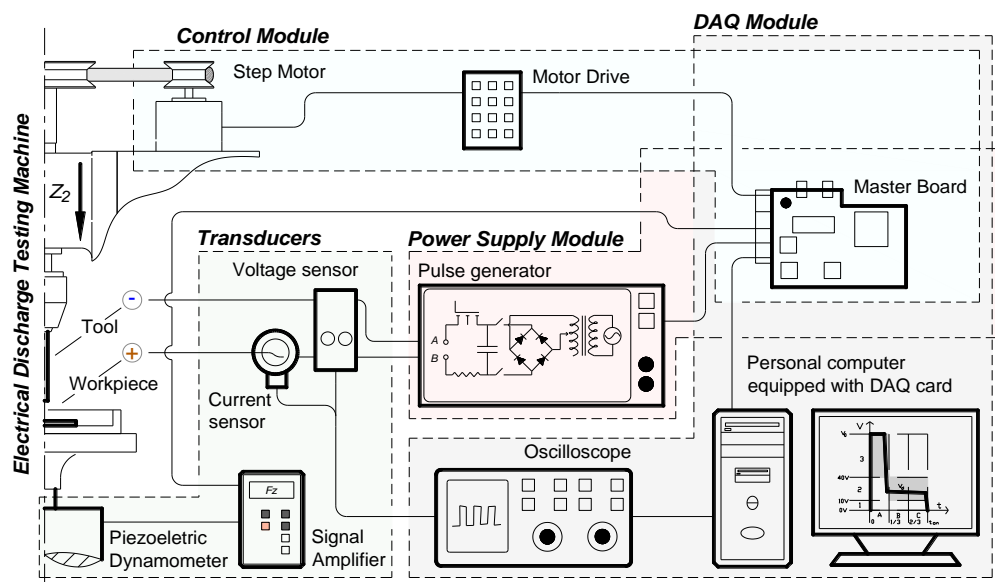
Figure 5 - Schematic representation of the hardware communication diagram of the experimental apparatus.
Source: Elaborated by the authors (2016).

(a)   (b)

Figure 6 - Single discharge testing machine; (a) Photograph of the custom-built apparatus, and (b) Photograph of the basic structural and kinematics appliances.
Source: Elaborated by the authors (2017).

3.2. Experimental Plan

The choice of material is of prime importance if investigations are expected to provide cleaner emission spectra from the plasma and to facilitate the input data calibration for the thermodynamic calculations. This requirement is important for enhancing the quantitative control upon the process, by limiting plasma contamination during the electrical discharge period. Unfortunately, the most commonly used engineering materials are unable to fulfil the above requirement, because of their complex physic and chemical interactions involving many different ions and alloying elements. In this research, workpieces were manufactured using unalloyed aluminium AA1050 and pure metals (Titanium 99.6%, Zinc 99.99%, Tin 99.999% and Aluminium 99.999%), due to purity of its composition. Tool electrodes were manufactured from the same materials in the AA1050 and Aluminium experiments reducing the potential influence of polarity. Tool electrodes were manufactured from electrolytic Copper (99.999%) for the pure metals experiments. The dielectric fluid, which plays an important role in defining the nature of the plasma, not only promotes cleaner plasma emission spectra, but it also favours the observation of the plasma during the single discharges. The AA1050 and Aluminium 99.999% experiments are performed using transparent and pure Millipore water droplets filling the gap between electrodes. This dielectric ensures reduced absorption and high transmission of radiation, favouring the observation of the plasma during the single discharges. An average dielectric strength of 8.2 MV/m is considered for the Millipore water, although this value can vary depending on the frequency of the electrical discharge. The pure metals experiments are performed using Fuchs EcoCut FEL Synth in order to facilitate electrical breakdown control. The electrodes were connected to a power source with a traditional point-to-plane electrode configuration. Direct polarity has been used with the plane as positive electrode and the point as negative electrode. The plane electrode was a rectangular plate (workpiece) of section 10x20mm with 5mm of thickness, while the point electrode was a round bar (tool) with 1mm diameter. The work tool position relative to the workpiece (gap) was fixed at 10 and 12μm.

The experimental observations shown some eroded craters without a perfectly round shape, sometimes surrounded by other small craters. This observation supports the idea that initial

irregular or indistinct workpiece surface conditions, residues and existing oxide layers can be responsible for poor interaction, leading to undesired non-axisymmetric plasmas. Therefore, the workpieces were polished before each test, facilitating the definition of single discharge patterns on the base materials, and the optical measurement of the craters boundaries. Even under laboratory controlled conditions, multi-crater formation occurs and cannot be detected promptly through the plasma electrical signature. As a result, each single experimental test was analysed individually, and those associated with abnormal craters and/or anomalous electrical signature were removed. The crater area was obtained through the calculated equivalent diameter of the eroded crater area.

In this research work, the main operating parameters are: (i) pulse time with values of 75, 150, 225 and 300µs, (ii) current intensity of 10A, (iii) gap with values of 10 and 12µm, (iv) direct polarity, and (vi) constant ionization voltage of 200V. The experiments are done randomly, minimizing systematic errors. From the experimental tests it is observed a slight variation in the voltage value, typically between 18V and 21V, depending on the test parameters.

4. RESULTS AND DISCUSSION

The formation of an eroded crater is result of the solid-plasma interaction. Its size and shape are evidences of the material removal mechanism, namely of the energy density of plasma channel, the time evolution observed for the plasma electrical resistivity and the plasma cross-sectional area, among other operating parameters. In what follows some experimental trends concerning crater morphology and its variation in time will be presented in a comprehensive manner to quantify the machinability of materials.

4.1. Topographical survey of the eroded craters

The morphology of the eroded craters is mainly characterised by a smooth bowl shape of minute dimensions and high radius-to-depth ratios. These eroded craters have a raised rim with the bottom surface at a much lower level than the surrounding surface in the range of few micrometres. These compact dimensions make the quantitative topographical survey of the eroded craters a very difficult task. Note that the impact of the electrical and materials parameters on the crater morphology can be assessed through its variation in time, as discussed before.

Figure 7 shows some eroded craters in pure metals for two different discharge times (75µs and 300µs). At the very early stages of the electrical discharge an eroded crater rapidly forms and continuously grows in time. In general, the crater diameter doubles their size with an increase of 4 in the time discharge. The craters eroded in the pure materials have a fairly circular geometry. However, Titanium seem to be the exception due to irregular shape, probably because its relatively scarce thermal conductivity. Analysing the eroded craters, it was observed that the Titanium presents uneven crater geometries, sometimes with multiple craters from a single discharge test. Most of the Tin and Zinc eroded craters have an almost perfect circular geometry with unusual internal axisymmetric rings (waviness). These eroded craters surface presents yet low roughness (almost polished aspect) compared with other experiments.

The eroded craters in both pure Aluminium and AA1050 showed irregular shapes accompanied by an unstable electrical signature during the discharge pulse. This irregular geometry is due to the great difficulty in the establishing of the plasma channel in these materials (Figure 8). The formation of aluminium oxide hinders the formation of the plasma having the craters a less perfect aspect when compared with the eroded craters in Titanium, Zinc and Tin.
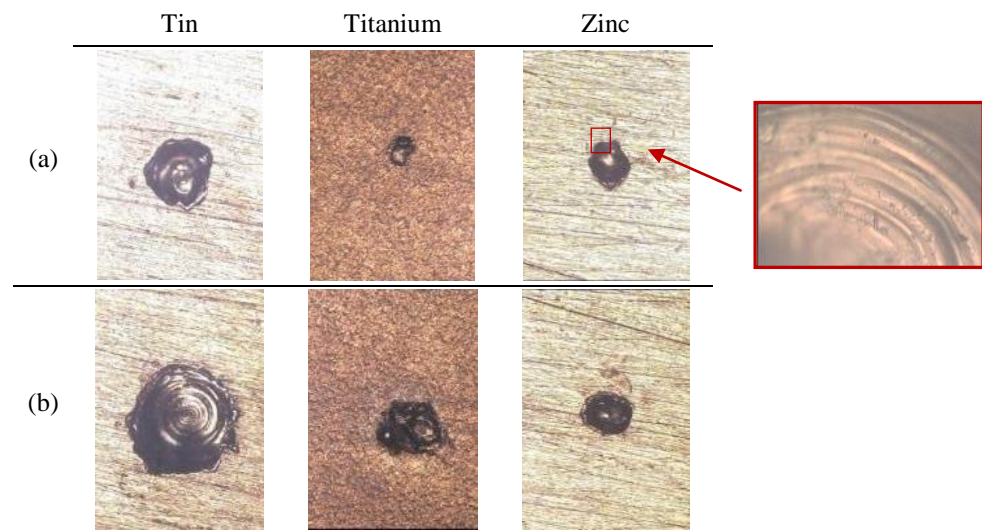
Figure 7 - Microscopic view of the eroded crater after the electrical discharge in Titanium, Tin and Zinc for different operating conditions; (a) gap of 10µm, current intensity of 10A and impulse time of 75µs, and (b) gap of 10µm, current intensity of 10A and impulse time of 300µs (equal magnification of 200x).
Source: Elaborated by the authors (2017).
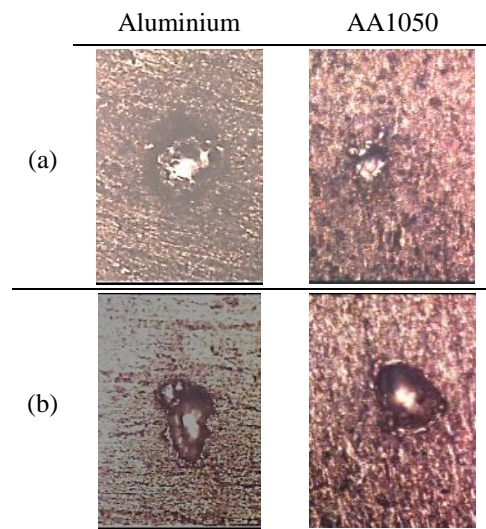
Figure 8 - Microscopic view of the eroded crater after the electrical discharge in pure Aluminium and AA1050 for different operating conditions; (a) gap of 10µm, current intensity of 10A and impulse time of 75µs, and (b) gap of 10µm, current intensity of 10A and impulse time of 300µs (equal magnification of 200x).
Source: Elaborated by the authors (2017).

Figure 9 and Figure 10 show measurements of the eroded craters diameter and craters depth in Titanium, Zinc and Tin as a function of the pulse time. At the very early stages of the electrical discharge an eroded crater forms and continuously grows in time. In general, the time evolution of the diameter and depth of the craters can be roughly fitted by a linear-law function. There are many sources of measurement error that in combination with a stochastic process can make difficult the interpretation of the experimental results. From Figure 9, it is clear that crater diameter increases from Titanium, Zinc to Tin. Some trend can be expected considering the melting point of each material. Since Titanium has the highest melting point (1930K) it is expected to have the smallest diameter for similar operating conditions (difficult to melt). In opposition, Tin has the lowest melting point (505K) and its eroded craters are those that present effectively the largest diameter. For Zinc, both crater diameter and melting point (693 K) present intermediate values between

Titanium and Tin. Figure 10 shows measurements of the eroded crater depth with a similar analysis of the experimental data. However, the depth values are less influenced than diameter values when the pulse time is increased.

Figure 11 shows measurements of the eroded crater diameter in pure Aluminium (99.999%) and AA1050 (99.5%) as a function of the pulse time. The influence of pulse time on the crater diameter is even more significant in the pure Aluminium than in the other pure metals. Additionally, a minor change in the percentage of the alloying elements can significantly influence the plasma-solid interaction. Indeed, from Equation 1 the discharge energy increases with the pulse time and then, a larger amount of material will be removed from the part. This fact is verified in the graphs presented. In all the materials, when increased the pulse time also the diameter tends to increase its value. Nevertheless, the melting point is only one of the physical properties of the material that influences the erosive process, this is a very important property as referred by Reynaerts (Reynaerts, 1997). Then, some conclusions as these can be drawn considering only this important parameter.
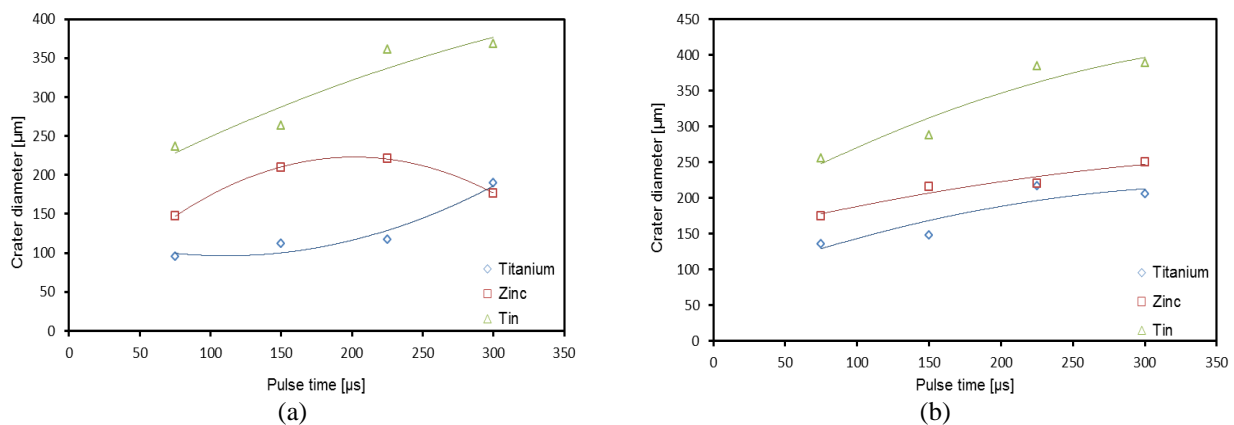
Figure 9 - Diameter of the eroded craters in Titanium, Zinc and Tin as a function of the pulse time for a gap of (a) 10µm and (b) 12µm.
Source: Elaborated by the authors (2017).
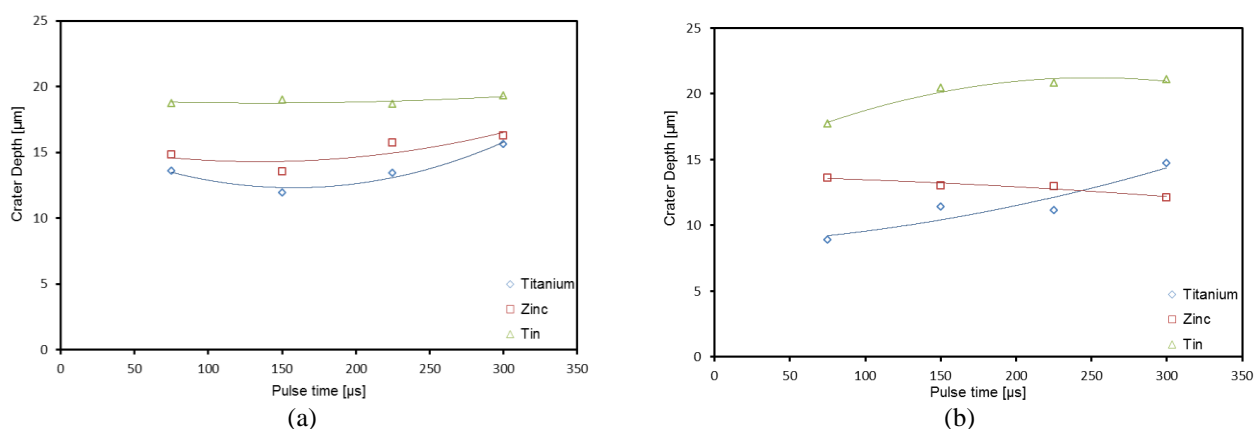
Figure 10 - Depth of the eroded craters in Titanium, Zinc and Tin as a function of the pulse time for a gap of (a) 10µm and (b) 12µm.
Source: Elaborated by the authors (2017).
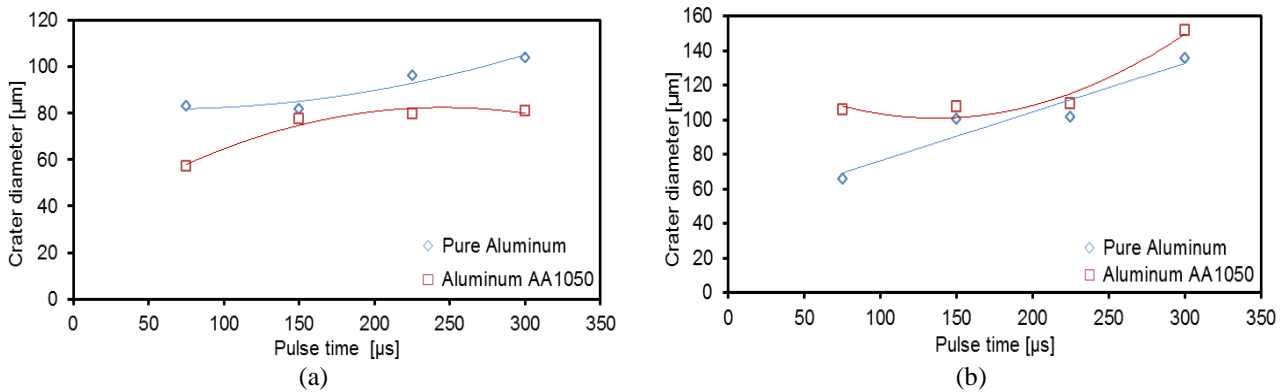
Figure 11 - Diameter of the eroded craters in pure Aluminium and AA1050 as a function of the pulse time for a gap of (a) 10μm and (b) 12μm.
Source: Elaborated by the authors (2017).

4.2. Morphology of the eroded crater

Figure 12 shows a schematic representation of the basic conceptual models for the eroded crater morphology. For the half spherical calotte model (Figure 12.a) it is possible to determine the ratio (R_1) of the diameter as a function of depth through the Equation 3, being this ratio a constant value (Dibitonto, 1989), (Salonitis, 2009) and (Popa, 2009). For the bowl plate model (Figure 12.b) it is also possible to determine the value of the ratio (R_2) through the Equation 4. However, in this case it was necessary to consider some practical values considered the gap value and average values of the cratear diameter (i.e gap of 10μm and crater diameter of 100μm) (Descoeudres, 2006) and (Bragança, 2013). Figure 13 compares the experimental morphology of the eroded craters with the estimated ratio obtained from Equation 3 and Equation 4 for the eroded craters in Titanium, Zinc and Tin. The theoretical-experimental correlational shows that none of these conceptual models fits with the experimental morphology. It is concluded with the values obtained that the crater diameter is substantially greater than the depth.
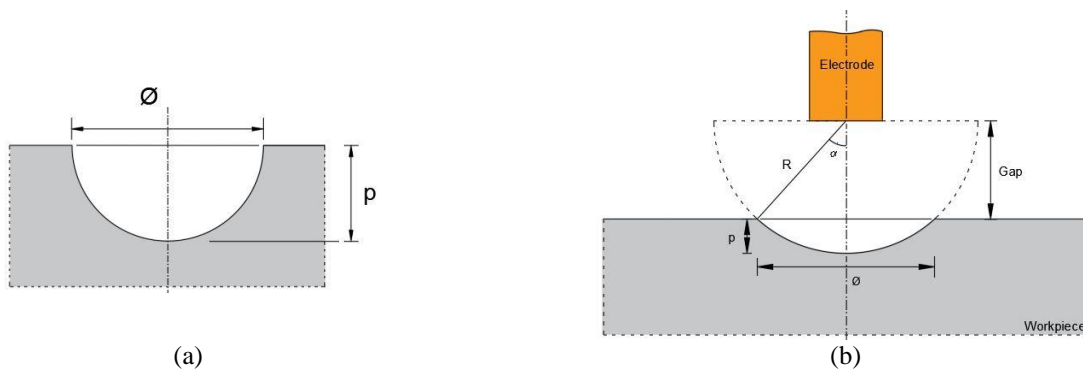
Figure 12 - Schematic representation of the eroded crater models; (a) half spherical calotte, (b) bowl plate.
Source: Elaborated by the authors (2017).

$$R_1 = \frac{\emptyset}{p} = \frac{\emptyset}{\frac{1}{2}\emptyset} = 2 \qquad \qquad [Eq. 3]$$

$$R_2 = \frac{\emptyset}{p} = \frac{2.sen(\alpha)}{1-cos(\alpha)} \sim [2;3] \qquad \qquad [Eq. 4]$$
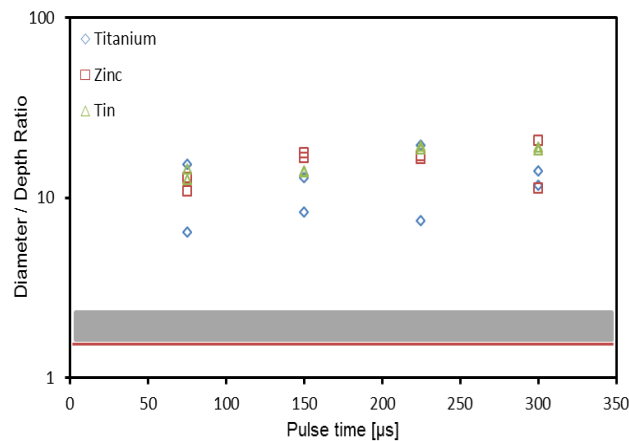
Figure 13: Ratio: diameter/depth of the eroded craters.
Source: Elaborated by the authors (2017).

5.3. Index of machinability

In order to compare the experimental observations with the index of Reynaerts (Reynaerts, 1997), it was calculated for each material its erosion specific energy. The erosion specific energy is determined by the energy per unit volume of material removal. Figure 14 shows evolutions of the specific erosion energy for Titanium, Zinc and Tin as a function of the pulse time. The almost constant values for each material is due to the more energy is supplied to the material, the more removed volume from it. The increasing trend in Zinc seems from some out-of-trend measurements.

Materials machinability can be estimated by the index of Reynaerts, C_m, then calculations are presented in Table 1. For the calculation of this index were used the physical properties of the material, which most influence machinability, according to Reynaerts (Reynaerts, 1997).

(a)   (b)
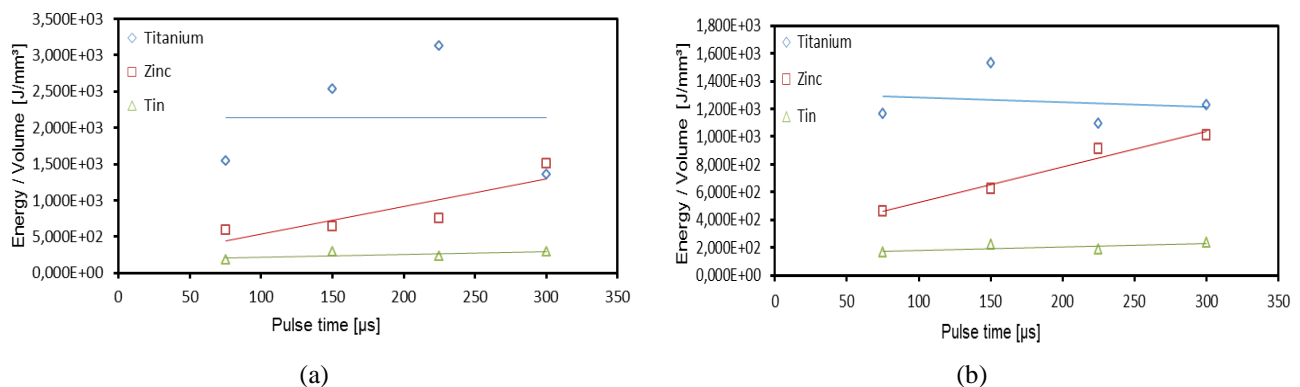
Figure 14 – Evolution of the ratio between the discharge energy and the removed volume as a function of the pulse time for a gap of (a) 10µm and (b) 12µm.

Considering the curves from Figure 14 and the indexes C_m from Table 1, it is possible to find a good correlation between the two machinability indexes. It is possible to observe that Tin has the lowest value followed by Zinc and Titanium. From this, Reynaerts index seems to be able to produce rapid and consistent estimates of the materials machinability for the EDM processes.

Table 1 - Index of machinability by erosion Cm.
Source: Elaborated by the authors (2017).

Materials / Properties	Titanium	Zinc	Tin
Melting point [K]	1930	693	505
Specific Heat [J/(Kg.K)]	528	390	256
Thermal Conductivity [W/(m.K)]	17	112,2	63,2
Density [Kg/m³]	4500	7100	7290
Index C_m [10^{10} J²/(m.s.Kg)]	3,343	2,101	0,412

5. CONCLUSION

As a first conclusion, it can be observed, that craters eroded in pure materials have a more uniform and constant geometry, when compared to allowed metallic materials used in engineering applications. Effectively, when the material is in the pure state, or near, the material removal mechanism by melting it becomes more regular and the craters formed in the material have an approximately circular geometry. In some cases, in pure materials with lowest melting points, craters with multiple axis-symmetric rings are formed. In general, in all materials when the pulse time increased, the volume of material removed also increased. It was also generally observed, that when the gap was increased, the diameter of the crater tended to increase as well, this being possibly explained with the expansion of the plasma channel.

Relatively to the values of the diameters and depths of the eroded craters, some conclusions can be drawn about the machinability of the materials. Considering the values obtained for the craters diameter, craters depth, index C_m and erosion specific energy, it can be expected that alloys constituted mainly by Titanium tend to be difficult to machine when comparing with Zinc and Tin. In fact, Tin is the easiest material to machine among the three. The values of the index C_m, when compared with the values obtained to the erosion specific energy are quite concordant among them. This leads to the conclusion that Reynaerts (Reynaerts, 1997) is correct in stating that the physical properties of the materials, which are the most important to be taken into account when machined by electro erosion are the specific heat, thermal conductivity and the melting point. In relation to pure and low-allowed aluminium studied, no conclusive evidences can be drawn. Because in the data obtained through the tests, it is not possible to determine a single trend. Being concluded that it was necessary a larger set of tests to determine the influence of the different elements on an alloy when machined by EDM.

Regarding the morphology which was found in experimentally eroded craters, it is possible to conclude that it is not in accordance with the models presented in the literature of the specialty, especially with the model of the half spherical calotte defended by several authors. The equation 5 presented in point 4 constitutes a better approximation to the real morphology, yet not exactly.

6. REFERENCES

ABDULKAREEM, S.; KHAN, A.; KONNEH, M. Reducing electrode wear ratio using cryogenic cooling during electrical discharge machining. **Int. Journal Advanced Manufacturing Technologies**, v.45, 2009.

BRAGANÇA, I.M.F.; ROSA, P.A.R.; DIAS, F.M.; MARTINS, P.A.F.; Alves, L.L. Experimental study of micro electrical discharge machining discharges. **Journal of Applied Physics**, v.113, n.23, 2013a.

BRAGANÇA, I.M.F.; RIBEIRO, G.R.; ROSA, P.A.R.; MARTINS, P.A.F. Prototype machine for micro-EDM. **In: Nontraditional Machining Processes**, London, Springer, p.153-76, 2013b.

DESCOEUDRES, A. **Characterization of electrical discharge machining plasma**. 2006. PhD Thesis, École Polytechnique Fédérale de Lausanne, France.

DIBITONTO, D.D.; EUBANK, P.T.; PATEL, M.R.; BARRUFET, M.A. Theoretical models of the electrical discharge machining process, a simple cathode erosion model. **Journal of Applied Physics**, n.66, 4095-4103, 1989.

EUBANK, P.; PATEL, M.; BARRUFET, M.; BOZKURT, B. Theoretical models of the electrical discharge machining process: the variable mass, cylindrical plasma model. **Journal of Applied Physics**, n.73, 1993.

LIU, Y.; ZHANG, Y.; JI, R.; CAI, B.; WANG, F.; TIAN, X.; DONG, X. Experimental characterization of sinking electrical discharge machining using water in oil emulsion as dielectric. **Materials and Manufacturing Processes**, v.28, n.4, p.355-63, 2013.

KANEMARU, M.; Sorimachi, S.; Ibuka, S.; Ishii, S. Single bubble generated by a pulsed discharge in liquids as a plasma microreactor. **Publishing Ltd Plasma Sources Science and Technology**, v.20, n.3, 2011.

KHAN, A. **Role of Heat Transfer on Process Characteristics During Electrical Discharge Machining**. 2011. PhD Thesis, International Islamic University, Malaysia,

KUNIEDA, M.; LAUWERS, B.; RAJURKAR, K.P.; SCHUMACHER, B.M. Advancing EDM through fundamental insight into the process. **Annals of the CIRP**, v.54, p.599-622, 2005.

LU, C.T. Influence of current impulse on machining characteristics in EDM. **Journal of Mechanical Science and Technology**, 2007.

POPA, M. Surface Quality of the EDM Processed Materials. **XIX IMEKO World Congress; Fundamental and Applied Metrology**, Lisbon, Portugal, September 6−11, 2009.

REYNAERTS, D.; HEEREN P.; VAN BRUSSEL H. Microstructuring of silicon by electro-discharge machining (EDM) - part I: theory. **Machine design Automation**, Belgium, Sensors and Actuators, v.A60, p.212-218, 1997.

SALONITIS, K.; STOURNARAS, A.; STAVROPOULOS, P.; CHRYSSOLOURIS, G. Thermal modeling of the matérial removal rate and surface roughness for die-sinking EDM. **The International Journal of Advanced Manufacturing Technology**, v.40, n.3, p.316-323, 2009.

SHUMACHER, B.M. After 60 years of EDM the discharge process remains still disputed. **Journal of Materials Processing Technology**, v.149, p.376–381, 2004.

YEO, S.H.; KURNIA, W.; TAN, P.C. Critical assessment and numerical comparison of electro-thermal models in EDM. **Journal of Materials Processing Technology**, v.203, n.1, p.241-251, 2008.

ZHANG, Y.; LIU, Y.; JI, R.; DONG, X. Research of the rheology of water-in-oil emulsion used in die-sinking EDM. **Chinese Journal of Mechanical Engineering,** Jixie Gongcheng Xuebao, v.47, p.188–93, 2011.